atmosphere

MDPI

Article

# The Spatial–Temporal Variation of Tropospheric $NO_2$ over China during 2005 to 2018

**Chunjiao Wang [1,2], Ting Wang [1,*] and Pucai Wang [1,2]**

[1] Key Laboratory of Middle Atmosphere and Global Environment Observation (LAGEO), Institute of Atmospheric Physics, Chinese Academy of Sciences, Beijing 100029, China
[2] University of Chinese Academy of Sciences, Beijing 100049, China
* Correspondence: wangting@mail.iap.ac.cn

Received: 4 June 2019; Accepted: 26 July 2019; Published: 1 August 2019


**Abstract:** In recent years, new and strict air quality regulations have been implemented in China. Therefore, it is of great significance to evaluate the current air pollution situation and effectiveness of actions. In this study, Ozone Monitoring Instrument (OMI) satellite data were used to detect the spatiotemporal characteristics of tropospheric $NO_2$ columns over China from 2005 to 2018, including spatial distribution, seasonal cycles and long-term trends. The averaged $NO_2$ pollution is higher in southeastern China and lower in the northwest, which are well delineated by the Heihe–Tengchong line. Furthermore, the $NO_2$ loadings are highest in the North China Plain, with vertical column density (VCD) exceeding $13 \times 10^{15}$ molec $cm^{-2}$. Regarding the seasonal cycle, the $NO_2$ loadings in eastern China is highest in winter and lowest in summer, while the western region shows the opposite feature. The amplitude of annual range increase gradually from the south to the north. If the entire period of 2005–2018 is taken into account, China has experienced little change in $NO_2$. In fact, however, there appears to be significant trends of an increase followed by a downward tendency, with the turning point in the year 2012. In the former episode of 2005–2012, increasing trends overwhelm nearly the whole nation, especially in the Jing–Jin–Tang region, Shandong Province, and Northern Henan and Southern Hebei combined regions, where the rising rates were as high as $1.0–1.8 \times 10^{15}$ molec $cm^{-2}$ $year^{-1}$. In contrast, the latter episode of 2013–2018 features remarkable declines in $NO_2$ columns over China. Particularly, the regions where the decreased degree was remarkable in 2013–2018 were consistent with the regions where the upward trend was obvious in 2005–2012. Overall, this upward–downward pattern is true for most parts of China. However, some of the largest metropolises, such as Beijing, Shanghai and Guangzhou, witnessed a continuous decrease in the $NO_2$ amounts, indicating earlier and more stringent measures adopted in these areas. Finally, it can be concluded that China's recent efforts to cut $NO_2$ pollution are successful, especially in mega cities.

**Keywords:** ozone monitoring instrument; tropospheric $NO_2$ columns; spatial distribution; temporal variation

## 1. Introduction

Nitrogen oxides ($NO_x$ = $NO_2$ + NO) are important trace gases in the atmosphere that have devastating impacts on the atmospheric environment and human health. In the lower troposphere, nitrogen dioxide ($NO_2$) plays a key role in air quality regulation and aerosols and ozone ($O_3$) formation [1]. $NO_2$ has a significant effect on atmospheric chemistry. $O_3$ is a secondary pollutant in the troposphere that is largely determined by the photochemical reactions of $NO_x$ and volatile organic compounds ($VOC_S$). On the other hand, a high level of $NO_x$ may likely combine with $VOC_S$ and other ultrafine particles and then produce photochemical smog and acid rain, respectively, further

affecting people's lives and health. Apart from these effects, $NO_x$ absorbs visible solar radiation and decreases atmospheric visibility, and to some extent, it affects global climate change [2,3]. As early as the 1960s, Barker et al. [4] proposed the maximum permissible concentration of $NO_x$ to be 0.5 mg/m$^3$ at any one time and 0.15 mg/m$^3$ for a 24 h average. In addition to the indirect impacts on the atmospheric environment, as a kind of strong toxic gas, $NO_2$ has more direct influences on public health. Large amounts of $NO_2$ are harmful to lung tissue and can lead to more respiratory diseases [5]. The World Health Organization (WHO) published Air Quality Guidelines (AQGs), which are aimed at reducing the detrimental effects of air pollution, while offering guidance to the public. The AQGs are focused on four main air pollutants: $O_3$, particulate matter (PM), sulfur dioxide ($SO_2$) and $NO_2$. The report suggested that guideline values were 40 μg/m$^3$ for annual $NO_2$ concentration and 200 μg/m$^3$ for 1 h $NO_2$ concentration. The report also indicated that different studies had inconsistent outcomes regarding the levels of $NO_2$ that could affect people. However, $NO_2$ was proved to be strongly associated with respiratory morbidity in adults and children because 70–90% of $NO_2$ can be absorbed from the respiratory tract of humans [6].

Troposphere $NO_2$ is produced by both anthropogenic and natural sources. The major sources, such as fossil fuel consumption, biomass burning, lightning or soil release, are common causes of $NO_2$ formation [7–9]. In addition, the existence of vehicles, power plants and some industries are also key factors in the $NO_2$ production. Some sources may also emit NO that could be spontaneously oxidized to $NO_2$ [10]. The highest $NO_2$ levels have been observed in the most populated and industrialized regions worldwide, such as eastern China, western Europe, the eastern US and India [11,12]. Nowadays, China is one of the fastest developing countries in the world, accompanied by simultaneously serious environmental pollution problems [13,14]. The strong increase in $NO_2$ pollution in China, especially over eastern China, is due to an increase in industrial development and traffic [15,16]. According to the Multi-resolution Emission Inventory for China (MEIC) [17], industry was the main source of $NO_2$ emissions over China in 2010, accounting for 39% of the total, followed by power plants and traffic, accounting for 32% and 25%, respectively, and residential sources occupied the lowest proportion [18]. Wintertime is a special period with the highest $NO_2$ concentrations because of the strong anthropogenic emissions in China, particularly with fossil fuels used for heating purposes.

Due to the importance of tropospheric $NO_2$ as it relates to the atmospheric environment and ecosystems, as well as human activity, it is essential to continually and accurately observe $NO_2$. However, there are only a limited number of observation stations in each country, and a complete worldwide ground monitoring network is still lacking, so it is difficult to obtain continuous and precise data for $NO_2$ from ground-based measurements. By contrast, satellite measurements can not only provide observations with global coverage but also provide information with high spatial and temporal resolutions. Global tropospheric $NO_2$ distributions are retrieved from the satellite instruments Global Ozone Monitoring Experiment (GOME, from 1995–2011) aboard ERS-2 [19,20], SCanning Imaging Absorption spectroMeter for Atmospheric ChartographY (SCIAMACHY, from 2002–2012) aboard the Envisat platform [21–23], Ozone Monitoring Instrument (OMI, since 2004) onboard Earth Observing System (EOS) Aura [24–26] and TROPOspheric Monitoring Instrument (TROPOMI, since 2017) aboard the Sentinel-5 Precursor [27]. A number of trend analyses studies have also been discussed [28–31]. Van der A et al. [32] investigated the tropospheric $NO_2$ concentration characteristics over China during 1996–2005 based on satellite data from GOME and SCIAMACHY and found that the tropospheric $NO_2$ columns were higher in densely populated and industrialized eastern China than in the western region, which has a sparser population density. Zhang et al. [33] reached the same conclusion. Moreover, the tropospheric $NO_2$ sources over China and the main factors affecting the growing trend are discussed in detail in their study. Lin and McElroy [34] found a notable reduction of $NO_x$ over China between late 2008 and mid-2009, which was mainly affected by the economic downturn and stringent regulations in Olympics. Georgoulias et al. [35] used several satellite data to study the long-term tropospheric $NO_2$ over the last two decades, which proved that tropospheric $NO_2$ was sensitive to socioeconomic changes and monotonous linear trends cannot be efficiently described for such long periods. OMI has been

providing observational results of various pollutant gases and greenhouse gases around the world and has been widely used to monitor and analyze $NO_2$ as well as other pollutants over China since 2004 [36–39]. In particular, the tropospheric $NO_2$ columns and total $NO_2$ columns over China during 2004 and 2010 were analyzed by Xiao et al. [40] and it was found that the two parameters presented adverse variations during the same season. The total $NO_2$ had the largest value in summer, while the tropospheric $NO_2$ had the smallest value. Wintertime showed the opposite results. Van der A et al. [41] noted that a distinct decreasing trend was visible in 2012. Ai [42], Cai [43] and Li [44] have been comprehensively analyzing the $NO_2$ concentrations in different regions of China over the last few years.

Recently the Chinese government has developed policies and plans to mitigate the adverse impacts of $NO_2$ and other greenhouse gases [45]. For example, the 12th five-year plan (2011–2015) set a goal to reduce $NO_x$ by 10% from 2011 to 2015 [46]. The 13th five-year plan (2016–2020) continues insisting upon the goal of energy conservation and emission reduction [47]. The Clean Air Alliance of China (CAAC) also released the Air Pollution Prevention and Control Action Plan in 2013 with the aim to improve the national air quality, especially in Beijing–Tianjin–Hebei, the Yangtze River Delta and the Pearl River Delta [48]. However, there are few studies addressing the variations in $NO_2$ over China after these control measures were implemented. In this study, we examine the changes in $NO_2$ at the tropospheric level over China between 2005 and 2018 obtained from OMI, including the spatial variations, long-term trends and monthly and seasonal cycles.

## 2. Data and Methods

### *2.1. OMI $NO_2$ Vertical Column Density (VCD) Product*

The Aura is a sun-synchronous near-polar orbit satellite from the National Aeronautics and Space Administration's (NASA) EOS. OMI is an important sensor onboard the EOS Aura satellite, which was launched on 15 July 2004. OMI is also inherited from GOME and SCIAMACHY and is combined with their advantages. OMI obtains daily measurements, which means the solar irradiance spectrum could be observed once per 24 h on a global scale, and now has provided more than 14 years of $NO_2$ data products, including total vertical column densities of $NO_2$ and stratospheric and tropospheric vertical column densities of $NO_2$ [49,50]. Furthermore, the high spatial resolution (13 km × 24 km) allows for more finer details of atmospheric parameters.

A differential optical absorption spectroscopy (DOAS) method has been validated to effectively retrieve the $NO_2$ slant column density (SCD) by OMI in the wavelength of 405–465 nm [51–53]. The accurate calculation of tropospheric $NO_2$ vertical column densities (VCD) depends on the SCD and the tropospheric air mass factor (AMF) [54,55]. Many studies have also proved the creditability of OMI $NO_2$ data products, and its accuracy can be accepted and used in $NO_2$ researches. For example, Celarier et al. [5] used ground and aircraft-based measurements to validate the OMI tropospheric $NO_2$ data and other principal quantities. The experimental results showed that the correlations between different instruments was 0.8–0.9. Lamsal et al. [56] compared OMI tropospheric $NO_2$ data with in situ aircraft, MAX-DOAS and ground-based direct sun Pandora measurements, respectively. OMI $NO_2$ data showed lower in urban areas and higher in remote regions. However, OMI retrievals generally were consistent with other methods, and the error was less than 20%. Ialongo et al. [57] present the comparison of NASA's OMI standard product (SP) and the Royal Netherlands Meteorological Institute (KNMI) DOMINO product with ground-based observations by the Pandora spectrometer in Helsinki. Results indicated that both satellite- and ground-based showed a similar behavior in weekly and seasonal cycles. These researches all add credibility in using OMI $NO_2$ data for air quality monitoring and analyzing. In this study, we focus on the study region of 4° N–60° N and 70° E–140° E, which covers nearly the entire area of China (see Figure 1), and we use the OMI Level-3 Global Gridded Tropospheric $NO_2$ Data Product (QA4ECV) from 2005 to 2018, compiled by the KNMI [58]. The datasets are processed with a spatial resolution of 0.125° × 0.125°, and the cloud radiance is less than 50%.

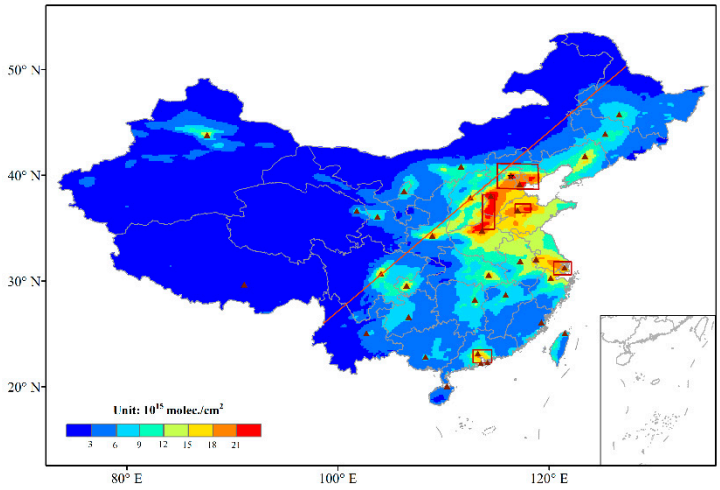


**Figure 1.** The spatial distribution of the average 14-year tropospheric $NO_2$ vertical column density (VCD) from 2005 to 2018 (unit: $10^{15}$ molec $cm^{-2}$). The red boxes denote the five hotspots we selected. From north to south, these hotspots are Beijing–Tianjin–Tangshan, South of Hebei and North of Henan combined, Jinan, Yangtze River Delta and Pearl River Delta. Triangles indicate the mean capital city of each province. The red line denotes the Heihe–Tengchong line (Hu Huaiyong line).

### *2.2. Meteorological Data Set*

Meteorological data were taken from Japanese 55-year Reanalysis (JRA-55) data, archived by the Japan Meteorological Agency. The data included total column precipitable water and temperature at pressure levels during the 14-year period. In addition, monthly means of wind speed data from the European Centre for Medium Range Weather Forecasts (ECMWF) were also used.

### *2.3. Trends Analysis Methods*

Two independent statistical methods, namely, the least squares regression and the F-test, were used to analyze the trends over China during different periods. According to the least squares regression, the $NO_2$ trend for each grid cell is assumed a Gaussian data distribution before calculating, and then it obtains the appropriate linear coefficient by linear fitting. In order to increase the robustness of the regression result, the F-test was performed after the calculation. An F-test is a homogeneity of variance test which is suitable for identifying the significance level of the linear trends. More details are given in Section 3.1. A trend is considered to be significant when the confidence level is above 95% for both least squares regression and the F-test [59].

## 3. Results and Discussion

### *3.1. Spatial Distribution and Long-Term Trends of Tropospheric $NO_2$ at the National Scale*

Figure 1 shows the 14-year average distribution of tropospheric $NO_2$ VCD over all of China from 2005 to 2018. Obviously, the $NO_2$ pollution in China is significant, and the distribution of tropospheric $NO_2$ is inhomogeneous. Previous studies have proven that $NO_2$ production is largely influenced by human activities, which means that areas with large population densities and high levels of industrialization may accumulate high concentrations of $NO_2$ [16]. The process of economic development and urbanization in the eastern region is much faster than in the western region in China, which explains why more serious $NO_2$ pollution prevails in the eastern part than in the western area of China. This characteristic can also be divided by the Heihe–Tengchong line (the line begins in the northeast city of Heihe and ends in Tengchong in the southwest). The Heihe–Tengchong line is a boundary that demonstrates the different population densities, as well as geographic and climatic characteristics of the areas [60,61]. The southeast area of the line is the most densely populated area, and

the area northwest of the line is sparsely populated. The North China Plain is the region over eastern China with the highest $NO_2$ columns. In addition, the Yangtze River Delta, Pearl River Delta, Sichuan Basin and Urumqi also have high levels of $NO_2$ columns located on both sides of the Heihe–Tengchong line. In addition, the capital city and nearly all the provincial capital cities, except Lhasa, have stronger $NO_2$ concentrations compared to the rest areas in each province.

In this study, as Figure 1 indicates, to better understand the changes and characteristics of the 14-year $NO_2$ concentrations over China in detail, we selected five areas with high $NO_2$ columns, namely Jing–Jin–Tang (38.8° N–41° N, 115° E–119° E), Northern Henan and Southern Hebei combined (35° N–38° N, 113.9° E–115° E), Jinan in the Shandong Province (36.6° N–37.3° N, 116.8° E–118.8° E), the Yangtze River Delta (30.8° N–23.4° N, 112.8° E–114.6° E) and the Pearl River Delta (22° N–23.4° N, 112.8° E–114.6° E); the 14-year mean tropospheric $NO_2$ VCD of the five hotspots are 13.46, 20.17, 18.85, 14.30 and 10.25 ($\times 10^{15}$ molec $cm^{-2}$), respectively.

As mentioned before, many environmental regulations have been implemented over China during 2005–2018. Since the 11th five-year plan put forward new proposals of emission reduction, more details of measures for air pollution prevention and control have been discussed. Some major regulations and policies during this period are listed in Table 1. As we can see, there are several essential policies promulgated in 2011, and then specifically implemented in 2012. Therefore, to access the effect of several measures and better explain the differences in the spatial variations of tropospheric $NO_2$ VCD, the year of 2012 was chosen as a turning point to divide the whole period into two stages. The tropospheric $NO_2$ VCD linear trends during the different stages over China are presented in Figure 2. Based on the OMI $NO_2$ data, a linear regression line was fit in each grid cell. Two stages were plotted, as shown in Figure 2a,b. Their significance levels were also shown in Figure 3a,b. Notably, an obvious and widespread increasing trend occurs in nearly the whole nation during 2005–2012, especially in the Jing–Jin–Tang region, Shandong Province, and Northern Henan and Southern Hebei combined regions, where the increased values were as high as 1.0–1.8 ($\times 10^{15}$ molec $cm^{-2}$ $year^{-1}$) ($p < 0.05$). In addition, the Yangtze River Delta, Chengdu–Chongqing zone, and Urumqi in the Xinjiang Province also showed a slight increase, with values ranging from 0.2 to 1.0 ($\times 10^{15}$ molec $cm^{-2}$ $year^{-1}$) ($p < 0.05$). In contrast, megacities such as Beijing, Shanghai and Guangzhou dropped significantly during this period, although their basic amounts of $NO_2$ column densities were still large. The change in Guangzhou was more prominent than those in the other two cities, with sharp declines of approximately −0.6 to −1.4 ($\times 10^{15}$ molec $cm^{-2}$ $year^{-1}$) ($p < 0.005$). This result is analogous to the previous study on the distribution analysis of $NO_2$ columns by Wang et al. [37,62].

**Table 1.** Major environmental regulations over China in recent years.

| Year of Implementation | Regulation | Main Goals | Reference |
|---|---|---|---|
| 2006–2010 | The 11th five-year plan | The $SO_2$ should be reduced by 10% from 2005 to 2010, but it lacks effective measures to reduce $NO_x$ emission. | Ma et al. [45] |
| 2011–2015 | The 12th five-year plan | The $NO_x$ should be reduced by 10% from 2011 to 2015. | Chinese National Government [46] |
| 2012 | Ambient air quality standards (GB3095-2012) | The concentration limitation of atmosphere $NO_x$ in China has been issued. | Van der A et al. [41] |
| 2013 | The Air Pollution Prevention and Control Action Plan | Aimed to improve the national air quality, especially in Beijing–Tianjin–Hebei, Yangtze River Delta and Pearl River Delta. | CAAC [48] |
| 2013–2017 | APPC-AP | $PM_{2.5}$ pollution has been paid more attention to. | Ma et al. [45] |
| 2016–2020 | The 13th five-year plan | It insists upon the goal of energy conservation and emission reduction. | Chinese National Government [47] |

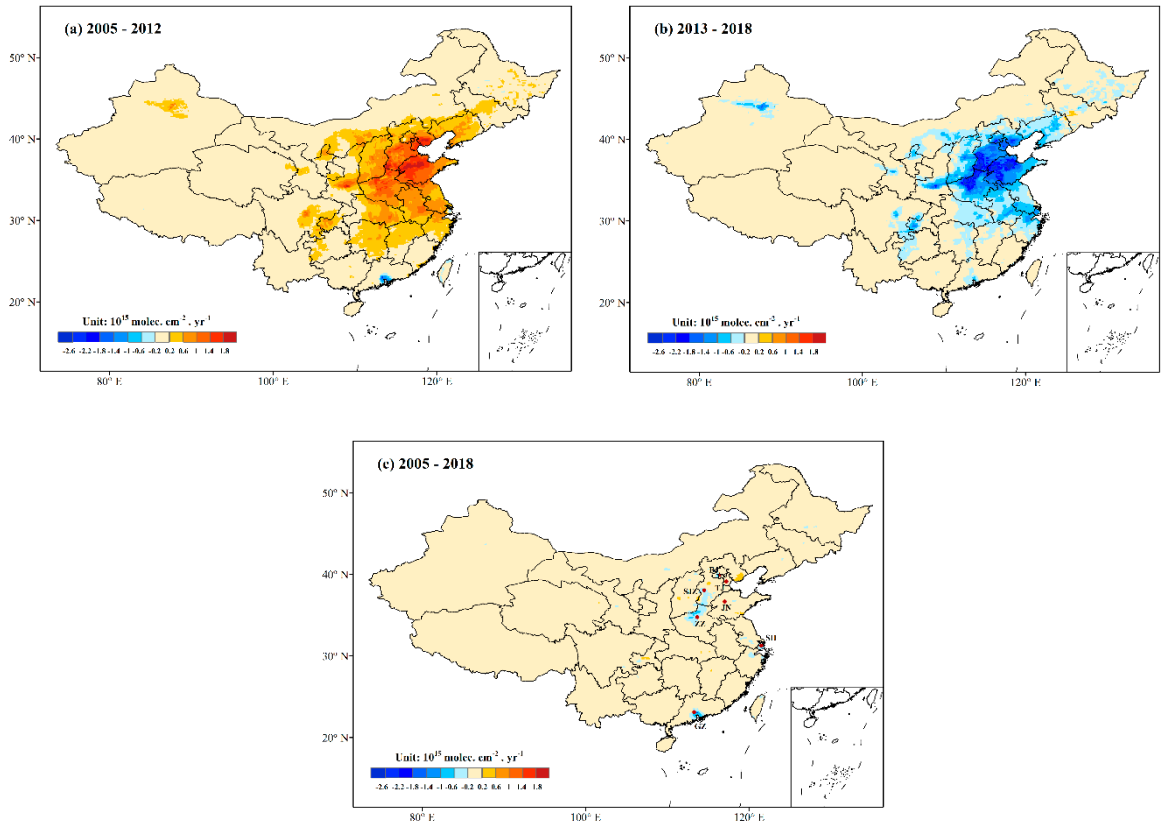


**Figure 2.** Tropospheric $NO_2$ VCD linear trends over China (unit: $10^{15}$ molec cm$^{-2}$ year$^{-1}$): (**a**) from 2005–2012; (**b**) from 2013–2018; and (**c**) from 2005–2018. The red dots denote the seven cities we discussed in Section 3.2. From north to south, these cities are Beijing, Tianjin, Shijiazhuang, Jinan, Zhengzhou, Shanghai and Guangzhou.).

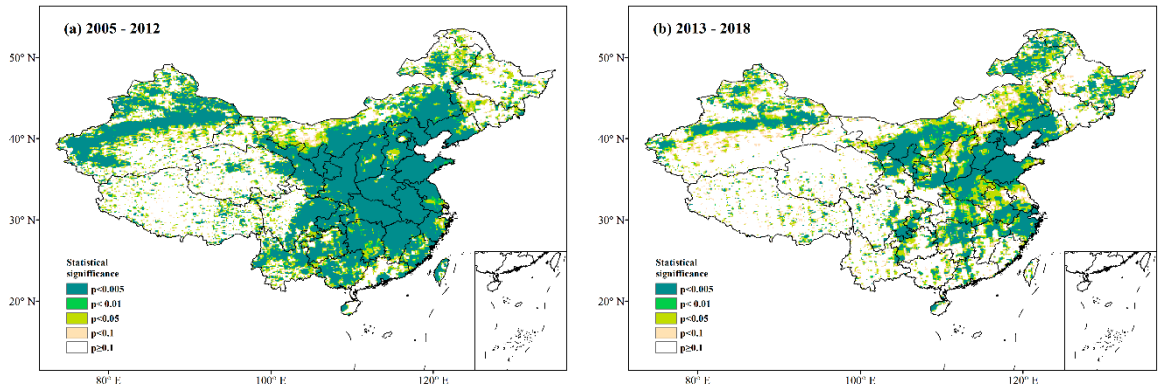


**Figure 3.** *Cont.*

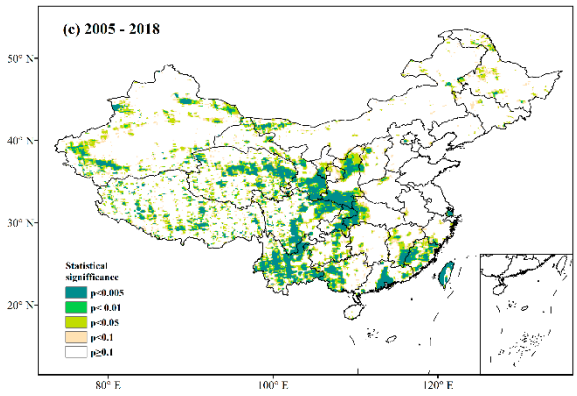


**Figure 3.** The significance levels of linear trends over China: (**a**) from 2005–2012; (**b**) from 2013–2018; and (**c**) from 2005–2018.

As shown in Figure 2b, the averaged densities of tropospheric $NO_2$ columns over China tended to decline markedly in most areas during the 2013–2018 period. In particular, the regions where the decreased degree was remarkable in 2013–2018 were consistent with the regions where the upward trend was obvious in 2005–2012, including the North China Plain, Yangtze River Delta, Chengdu–Chongqing zone, Pearl River Delta and Urumqi (all $p < 0.05$). Additionally, the trends in the megacities of Beijing, Shanghai and Guangzhou remained downward. However, the decline in Guangzhou had slowed compared with the previous stage (2005–2012), with values of approximately −0.2 to −0.6 ($\times 10^{15}$ molec $cm^{-2}$ $year^{-1}$) in this period.

Subsequently, the overall linear trend and their significance levels over China during the 14-year period are shown in Figures 2c and 3c. Overall, the $NO_2$ concentrations in megacities such as Beijing, Shanghai and Guangzhou have decreased substantially, especially the Guangzhou in the Pearl River Delta. Although the significance levels are not significant in many areas, confidence levels in these cities are all above 95% ($p < 0.05$). It means that environmental protection measures have been effectively implemented and have had some effects in these regions. Simultaneously, there was also a significant reduction in the combined Northern Henan and Southern Hebei region. In contrast to these areas, a few cities and regions such as Tangshan and the main cities of Chongqing had an increased trend to a small extent. Most of the remaining regions were maintained in a stable state without remarkable fluctuations during the 14-year study period.

### *3.2. Spatial Distribution and Long-Term Trends of Tropospheric $NO_2$ VCD at the Five Hotspots*

The annual variations in the five hotspots present different change patterns in Figure 4. The mean tropospheric $NO_2$ VCD in Jing–Jin–Tang, the combined Southern Hebei and Northern Henan (S. Hebei and N. Henan), Jinan, Yangtze River Delta and Pearl River Delta from 2005–2018 are 13.46, 20.17, 18.85, 14.30 and 10.25 ($\times 10^{15}$ molec $cm^{-2}$), respectively, as mentioned in Section 3.1. The S. Hebei and N. Henan combined region has a maximum value in the 14-year average of $NO_2$ VCD, followed by Jinan, and the minimum is in the Pearl River Delta, which is consistent with the overall change in $NO_2$ columns for the five main areas over the 14 years (see Figure 4). More specifically, S. Hebei and N. Henan were the regions with the highest $NO_2$ columns until 2010, after which the highest value region swung back and forth between S. Hebei and N. Henan combined and Jinan, but both areas were higher than any other regions. Moreover, the annual changes in the S. Hebei and N. Henan combined region, Jinan and Jing–Jin–Tang are similar during the 14-year study period. The tropospheric $NO_2$ VCD in the three regions increased significantly from 2005 to 2007, decreasing by 7.7%, 3.6% and 18.2%, respectively, in 2008. The reduction is closely related to a series of policies issued by the government during the 2008 Olympic Games, for instance, restrictions were imposed on traffic and emission reductions were expected for industrial activities, especially in Beijing and the surrounding cities [34,63]. Increasing trends with different levels appeared in the three regions during 2008–2011.

However, the three regions have all shown a decreasing trend in recent years, where the $NO_2$ VCD in the S. Hebei and N. Henan combined region, Jinan and Jing–Jin–Tang has decreased by 42.6%, 51.1% and 33.4%, respectively, since 2011.

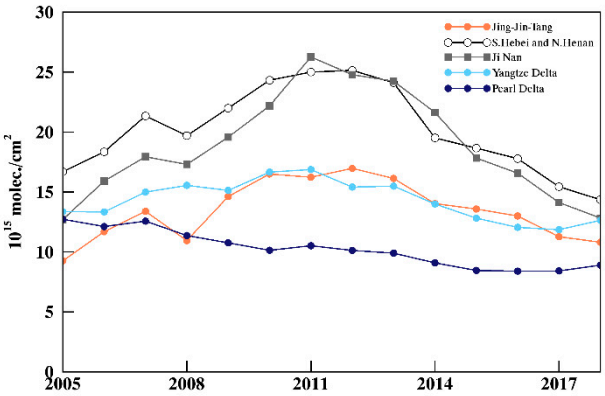


**Figure 4.** Annual variations in tropospheric $NO_2$ VCD in the five hotspots we selected during 2005–2018. (unit: $10^{15}$ molec cm$^{-2}$).

By comparison, annual variations in the other two regions are relatively moderate, and the $NO_2$ column concentrations are also comparatively smaller. The tropospheric $NO_2$ VCD fluctuated over a small range in the Yangtze River Delta during 2005–2011 (increased by 26.3%), with a peak at $16.87 \times 10^{15}$ molec cm$^{-2}$ in 2011 and a subsequent, steady decline (decreased by 25.1% since 2011). The mean $NO_2$ VCD dropped slowly in the Pearl River Delta during the 14-year period and decreased by 30.1% during this period. In brief, the tropospheric $NO_2$ VCD in the five hotspots, except the Pearl River Delta, experienced a process of first increasing and then decreasing, and this process is not simply monotonous.

Table 2 shows the variations in tropospheric $NO_2$ columns over some leading cities in the five areas we selected. The locations of these cities can be found in Figure 2c. Nearly all cities except Guangzhou had a growth of $NO_2$ in 2012 compared with 2005 and then declined until 2018. Compared with 2005, the amount of $NO_2$ in Jinan, Tianjin, Beijing, Zhengzhou and Shijiazhuang increased more obviously in 2012 and increased by 95.1%, 71.0%, 65.9%, 61.7% and 50.1%, respectively. By contrast, compared with 2012, all cities showed a downward trend in 2018, especially the cities with an obvious upward trend in the previous stage (2005–2012). Guangzhou was a more special situation that decreased in these two periods. In addition, Beijing had the lowest concentration of $NO_2$ among these cities.

**Table 2.** The change in tropospheric $NO_2$ columns over some leading cities in high concentration regions during 2005–2018. (unit: $10^{15}$ molec cm$^{-2}$).

| City | 2005 | 2012 | 2018 | Rate of Change (2005–2012) (%) | Rate of Change (2012–2018) (%) |
|---|---|---|---|---|---|
| Beijing | 9.62 | 15.96 | 9.99 | 65.9 | −37.4 |
| Tianjin | 14.25 | 24.37 | 15.57 | 71.0 | −36.1 |
| Shijiazhuang | 14.32 | 21.50 | 14.20 | 50.1 | −34.0 |
| Zhengzhou | 14.94 | 24.16 | 13.01 | 61.7 | −46.2 |
| Jinan | 12.70 | 24.78 | 12.83 | 95.1 | −48.2 |
| Shanghai | 11.82 | 12.77 | 10.63 | 8.0 | −16.8 |
| Guangzhou | 14.48 | 10.85 | 9.23 | −25.1 | −14.9 |

In fact, except for the policies enforced in 2008, the government has also proclaimed some measures and plans to prevent or control air pollution. As mentioned before, the 12th five-year plan implemented in 2012 and the Air Pollution Prevention and Control Action Plan implemented in 2013 are important

policies for environmental governance in China. The changes in $NO_2$ amount over China can also reflect the effectiveness of these policies to a certain extent.

Beijing, as the capital of China, is the political and cultural center of China. Beijing is also an area where various environmental protection policies are strictly implemented. Therefore, it is necessary to explore the effects of environmental governance. The detailed variation characteristics of the tropospheric $NO_2$ VCD in Beijing and Jing–Jin–Tang were analyzed as follows. Figure 5a shows the 14-year averaged $NO_2$ VCD in Beijing and the Jing–Jin–Tang region (12.58 and 13.46 × $10^{15}$ molec $cm^{-2}$, respectively). It is evident that Beijing, Tianjin and Tangshan are major cities in the Jing–Jin–Tang region, all of which are characterized by high concentrations of $NO_2$. Furthermore, the linear trend is reflected in Figure 5b. Compared with other areas in the Jing–Jin–Tang region, Beijing showed a significant downward trend during the 14-year study period, approximately −0.042 (×$10^{15}$ molec $cm^{-2}$ $year^{-1}$) after the regional average. However, the Jing–Jin–Tang region had an opposite tendency, approximately 0.060 (×$10^{15}$ molec $cm^{-2}$ $year^{-1}$) after the regional average. This result was mainly ascribed to the other areas in this region, especially Tangshan, which exhibited relatively strong growth trends.

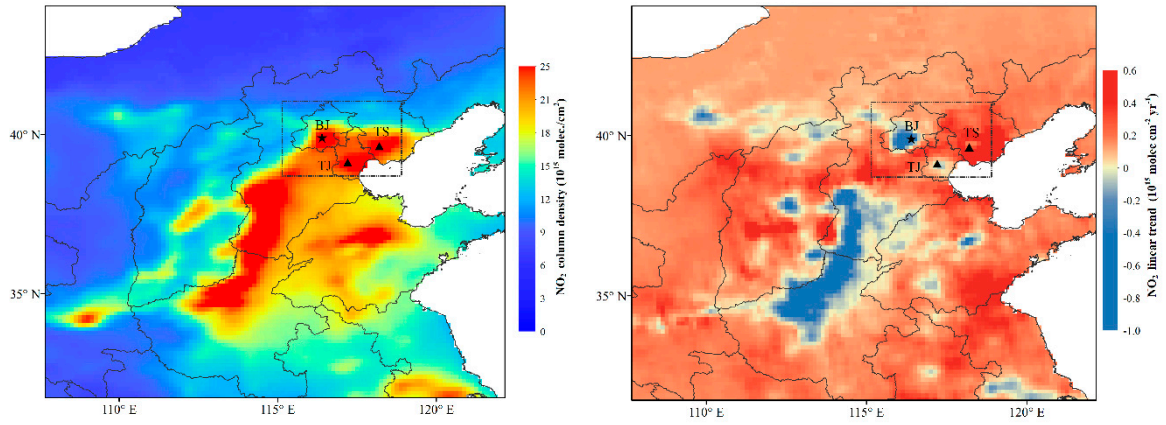


**Figure 5.** (**a**) Tropospheric $NO_2$ VCD in Beijing and Jing–Jin–Tang averaged from 2005 to 2018 (unit: $10^{15}$ molec $cm^{-2}$) and (**b**) tropospheric $NO_2$ VCD linear trends in Beijing and Jing–Jin–Tang from 2005 to 2018 (unit: $10^{15}$ molec $cm^{-2}$ $year^{-1}$). The black boxes denote the locations of Beijing and the Jing–Jin–Tang region. Triangles indicate the three cities (Beijing, Tangshan and Tianjin).

Monthly variations in $NO_2$ column densities in Beijing and the Jing–Jin–Tang region during the 14-year study period are presented in Figure 6a. First, an outstanding feature is revealed, where the variation in $NO_2$ VCD shows a periodic seasonal cycle, with the highest values in winter and lowest in summer. This feature will be discussed in depth in Section 3.3. Second, the long-term trends in the two regions are described. The $NO_2$ amount in Beijing is close to that of the Jing–Jin–Tang region every month, but the downward trend of the former is more obvious than the latter over the past 14 years. This characteristic is more evident in Figure 6b.

As Figure 6b depicts, the trends in the $NO_2$ VCD in Beijing basically coincide with the Jing–Jin–Tang region. The values of $NO_2$ VCD in Beijing were lower than those of Jing–Jin–Tang nearly every year, except in 2005 and 2006. Specifically, the two regions featured increasing $NO_2$ from 2005 to 2007 and showed a significant drop in 2008 (decreasing by 20.4% in Beijing and 18.2% in Jing–Jin–Tang), mainly due to the pollution control regulations during the Olympic Games. From 2008 to 2012, Beijing and Jing–Jin–Tang showed an upward trend, reaching a maximum in 2012 (increasing by 54.5% and 55%, respectively, since 2008), and then, a steady downward trend has been sustained in recent years (decreasing by 37.4% and 36.2%, respectively, since 2012). Overall, the $NO_2$ amount in Beijing

has decreased by 3.8% since 2005, while the $NO_2$ amount in Jing–Jin–Tang has increased by 14.3% since 2005.

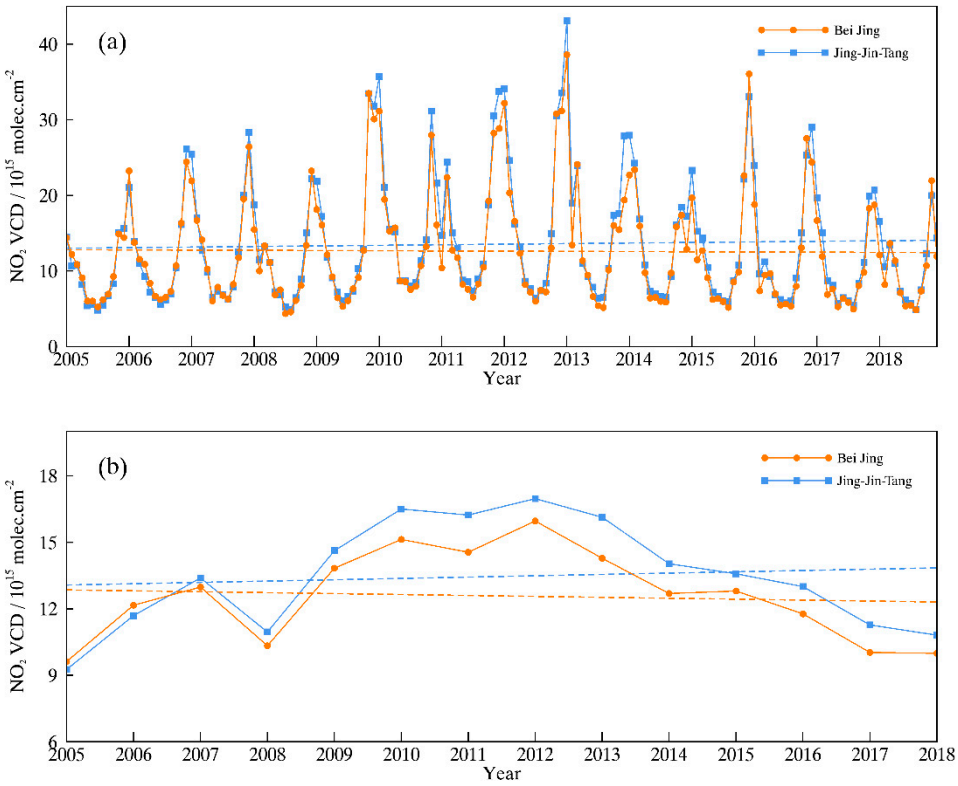


**Figure 6.** (**a**) Monthly variations in the tropospheric $NO_2$ VCD in Beijing and Jing–Jin–Tang from January 2005 to December 2018 (unit: $10^{15}$ molec $cm^{-2}$); (**b**) Yearly averaged variations in tropospheric $NO_2$ VCD in Beijing and Jing–Jin–Tang from 2005 to 2018 (unit: $10^{15}$ molec $cm^{-2}$).

Beijing and its surrounding areas differ greatly in their variations in $NO_2$ columns, which may be due to the following reasons: On the one hand, Beijing has implemented stricter environmental control policies, including motor vehicle management and factory relocations since 2008, which has fundamentally curbed the emissions of $NO_x$. This inference is affirmed by Diao et al. [64]. However, $NO_2$ has a short life, especially in summer, so pollutants cannot be transported over long distances. Accordingly, the distributions of $NO_2$ are associated with emission sources and meteorological conditions [63].

### *3.3. Monthly and Seasonal Patterns of Tropospheric $NO_2$ VCD*

The seasonal distributions of $NO_2$ VCD over China over 14 years are shown in Figure 7. The seasonal variation features are noticeable throughout the country, where east China is the highest in winter and lowest in summer. In contrast, west China is the highest in summer and lowest in winter (except Urumqi). This difference is probably due to the differences in the generation of $NO_x$ in different regions. Van der A et al. [32] concluded that the main sources of $NO_x$ in the western part of China were natural emissions, which were dependent on temperature, soil and precipitation, while the $NO_x$ in eastern China was mainly related to human activities such as industrial emissions. In particular, coal-fired heating is a prime reason for large $NO_x$ emissions during wintertime. The $NO_x$ lifetime is longer in winter than in other seasons, causing severe air pollution at this time. In addition, the areas with high concentrations of $NO_2$ are consistent with the areas of focus in Figure 1.

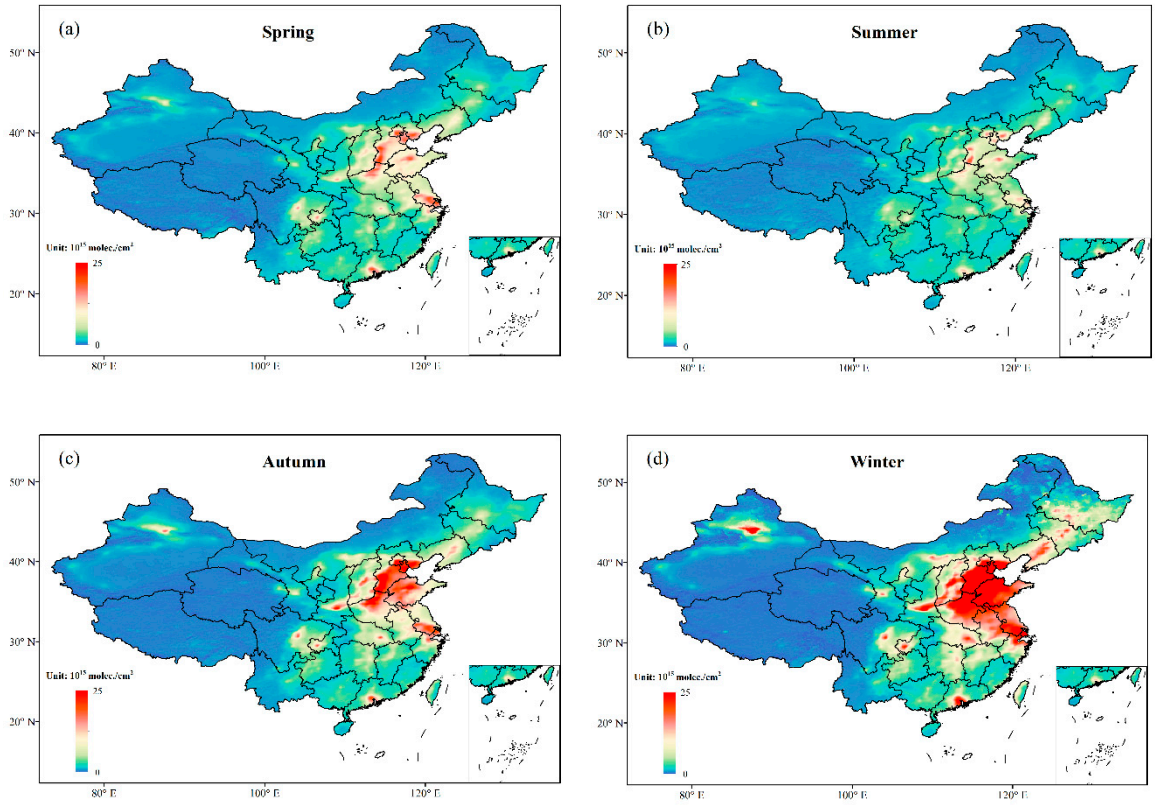


**Figure 7.** Seasonal $NO_2$ column over China during 2005–2018 (unit: $10^{15}$ molec $cm^{-2}$): (**a**) spring; (**b**) summer; (**c**) autumn; and (**d**) winter.

The analyses of time series are based on monthly averages and seasonal averages, which are shown in Figure 8. Monthly averages of $NO_2$ VCD were calculated in five areas during the 14-year period and drawn in Figure 8a. Regardless of the regions we considered, winter (January, February and December) showed higher values than summer (June, July and August), forming a "V" shape in each chart. Moreover, annual range is the most evident in the S. Hebei and N. Henan combined region as well as in Jinan, where maximum minus minimum values exceed 25 ($\times 10^{15}$ molec $cm^{-2}$) in different months. Then, the Jing–Jin–Tang and Yangtze River Delta values are more than 15 ($\times 10^{15}$ molec $cm^{-2}$) regarding the difference between winter and summer. In contrast, the Pearl River Delta has the smallest amplitude in both numerical value and annual cycle, with the highest value in January and lowest value in August along with difference values of less than 5 ($\times 10^{15}$ molec $cm^{-2}$).

In Figure 8b, each chart depicts seasonal comparisons of the five regions during the whole period. The characteristics of long-term seasonal variations were remarkable in winter and autumn but were not obvious in summer and spring among the five specified regions for the 2005–2018 period. In winter, the S. Hebei and N. Henan combined region and Jinan had the maximum values of tropospheric $NO_2$ VCD of the entire period. These regions also showed the most dramatic variability. The temporal patterns in the two regions were similar to those of the analysis we completed in Figure 4. For the Jing–Jin–Tang region, the changes in the $NO_2$ amount during winter showed an increasing trend before 2009 and then a decreasing trend until 2018, except for the abnormal peak in 2010. The reduction rate of tropospheric $NO_2$ VCD between 2011 and 2014 was larger than that between 2014 and 2018. In contrast, the changes in tropospheric $NO_2$ columns in the Yangtze River Delta and Pearl River Delta were slight in winter during the 14-year period, and the $NO_2$ amounts in the former region were all higher than those in the latter period of each year. The variations in tropospheric $NO_2$ columns in autumn during the 14-year period were somewhat similar to those in winter. However, the $NO_2$ levels were smaller than those in winter.

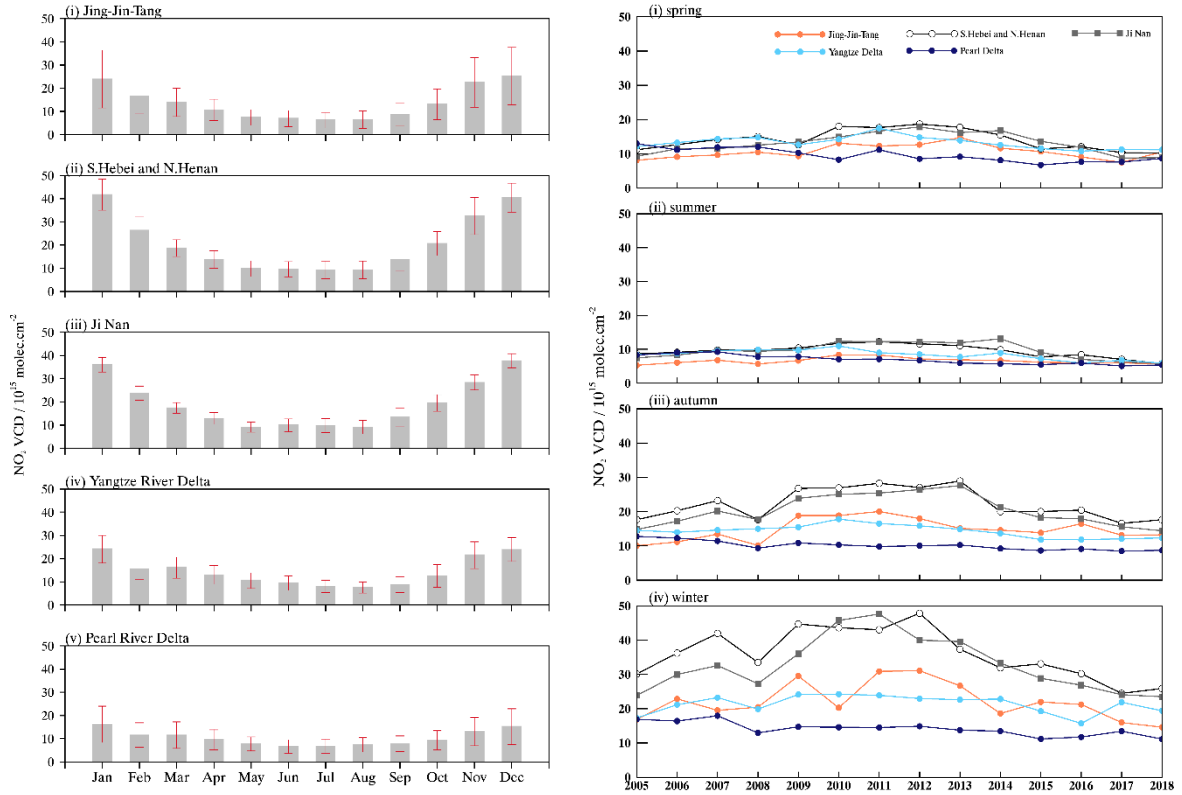


**Figure 8.** (**a**) Monthly $NO_2$ column averages in five hotspots during 2005–2018 (unit: $10^{15}$ molec $cm^{-2}$), with error bars representing the standard error; and (**b**) variations in the seasonally averaged columns in five hotspots during 2005–2018 (unit: $10^{15}$ molec $cm^{-2}$).

Similarly, a more detailed comparison and analysis of the seasonal variations between Beijing and Jing–Jin–Tang was carried out. As clearly shown in Figure 9a, conspicuous differences in the $NO_2$ amount between Beijing and Jing–Jin–Tang occurred in January, February and December, and the difference values were approximately 3.06, 6.94 and 2.56 ($\times 10^{15}$ molec $cm^{-2}$), respectively. During other months, there were only subtle differences in $NO_2$ amounts between the two regions. This point is more evident in Figure 9b. Compared with other seasons, the long-term changes in the $NO_2$ columns in winter were the most significant; an intense contrast between the two regions was also apparent. In the past 14 years, the values of the $NO_2$ columns in Beijing were basically smaller than those in Jing–Jin–Tang. Furthermore, the $NO_2$ concentrations in both places have steadily decreased during winter since 2012. With the implementation of various measures, $NO_2$ pollution has been more effectively controlled in Beijing than in the surrounding areas. In recent years, Beijing has taken more stringent measures to control air pollution during the winter heating period. The government has focused on key emission sources during autumn and winter, and several measures were proposed, including promoting the adjustment of transportation structure and encouraging investments in new high-technology industries such as clean energy.

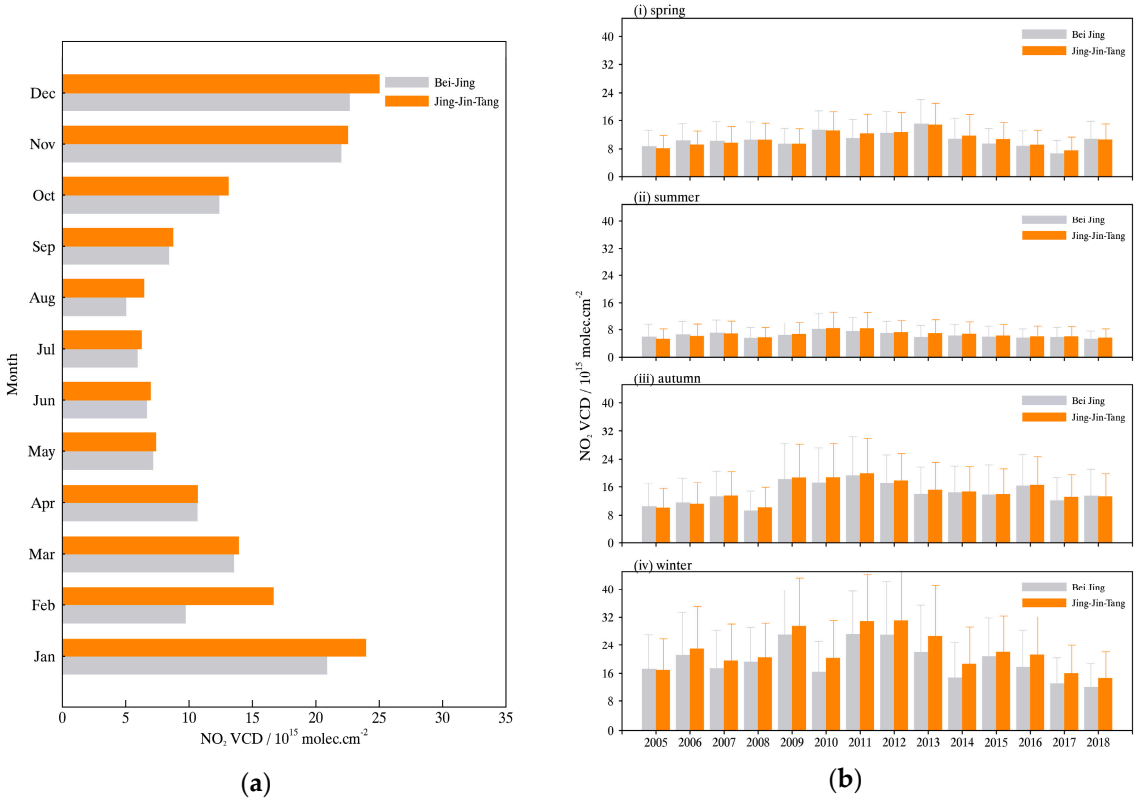


**Figure 9.** (**a**) Monthly averages in $NO_2$ columns in Beijing and Jing–Jin–Tang during 2005–2018 (unit: $10^{15}$ molec $cm^{-2}$); and (**b**) seasonal variations in $NO_2$ columns in Beijing and Jing–Jin–Tang during 2005–2018 (unit: $10^{15}$ molec $cm^{-2}$), with error bars representing the standard error.

### *3.4. Impacts of Meteorological Conditions*

Generally, three main factors need to be considered to explain the $NO_2$ changes in a specific region, including the amount of $NO_x$ emission, $NO_x$ lifetime and the $NO_2$ transportation among diffident regions [62]. As discussed in Section 3.3, $NO_2$ variation has a significant seasonal characteristic, which is larger in winter and lower in summer. First, from the perspective of $NO_x$ emission, large increase in fossil fuel consumption is a prime reason due to large $NO_x$ emissions during wintertime. Then in winter, the lifetime of $NO_x$ is also larger than other seasons because of the weaker solar radiation and lower atmospheric temperature. All these factors delay the process of atmospheric chemical reactions. In contrast, the solar radiation is stronger in summer and chemical reaction is active, which are beneficial to $NO_2$ removal. Finally, $NO_2$ transportation is related to meteorological conditions. In winter, although the average wind speed is higher, the $NO_2$ emissions are also larger. In addition, the atmospheric boundary layer is low in winter. It is easy to form an inversion layer, which leads $NO_2$ remaining in the lower troposphere.

To further analyze the different monthly variations in different regions, we decided to investigate the meteorological conditions in these five areas. Figure 10 illustrates the annual cycle of precipitable water, wind speed and temperature at the five hotspots. Combined with the monthly average variations of $NO_2$ in Figure 8a, it is obvious that $NO_2$ monthly variation is associated with the seasonal change of meteorological conditions. Temperature and precipitable water are colder and less in winter which could weaken the rate of oxidation and wet deposition. In addition, compared with Jing–Jin–Tang, the S. Hebei and N. Henan combined region and Jinan, the Yangtze River Delta and the Pearl River Delta show distinct meteorological conditions. Both two regions are located at low latitudes in the Southern China and near the ocean, with average temperatures higher than other three areas. Moreover, with monsoon influence, there are more precipitation in the two regions, which are all beneficial to

$NO_2$ eliminated. This result is also consistent with the seasonal variations of $NO_2$ concentration in the five hotspots.

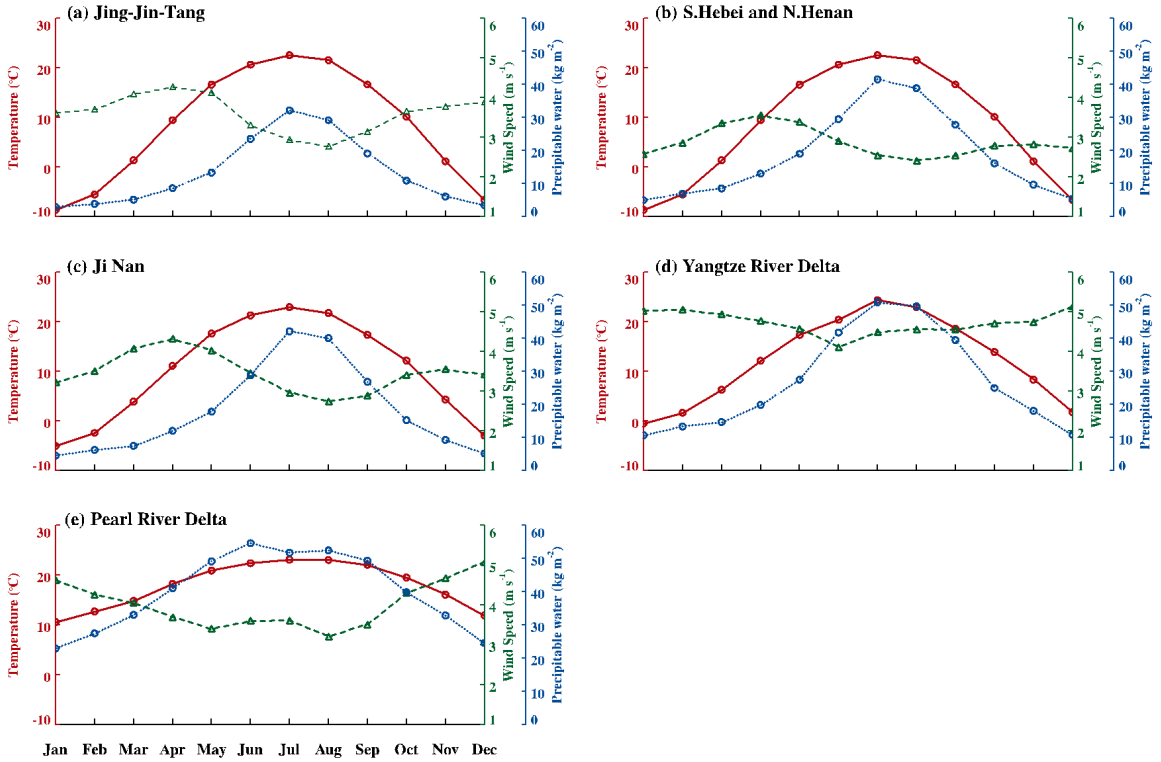


**Figure 10.** Annual cycle of precipitable water (unit: kg $m^{-2}$), wind speed (unit: m $s^{-1}$) and temperature (unit: °C) at 975 hPa in five areas.

## 4. Conclusions

In recent years, some new measures that can improve and prevent air contamination have been implemented in China. It is of great significance to understand the current air pollution situation by exploring the changes in $NO_2$ concentrations. Furthermore, these new measures can also evaluate the beneficial effects of pollution policies and provide some reference for the next steps in air pollution control. Therefore, the results of this study describe the characteristics of tropospheric $NO_2$ in terms of spatial distributions and temporal variations from 2005 to 2018 over China using OMI satellite data. The main conclusions are summarized as follows:

(1) The $NO_2$ pollution in China is significant, and the distribution of tropospheric $NO_2$ VCD is uneven. This pollution is higher in southeastern China and lower in the northwest, which is well divided by the Heihe–Tengchong line. In addition, the North China Plain is the region over eastern China with the highest $NO_2$ columns. Then, five areas with high $NO_2$ columns in southeast China were selected for detailed discussion, including Jing–Jin–Tang, the combined regions of Northern Henan and Southern Hebei, Jinan in the Shandong Province, Yangtze River Delta and Pearl River Delta.

(2) $NO_2$ concentrations show long-term variability that varies regionally. On the one hand, the concentration of $NO_2$ in the Pearl River Delta has been in a slow but steady decline apart from slight increases in 2007 and 2010. On the other hand, the annual variation in the $NO_2$ columns displays two different stages in the other four areas. First, the $NO_2$ amounts in these four regions increased significantly until 2011 or 2012, except in 2008, due to the strict measures taken for the Olympic Games. Subsequently, the growth of $NO_2$ VCD has slowed down in recent years.

Moreover, some of the largest metropolises in China, such as Beijing, Shanghai and Guangzhou, show a downward trend in the $NO_2$ amounts during the 14-year study period.

(3) The characteristics of the seasonal cycle are obvious in China. The $NO_2$ amount in eastern China is the highest in winter and lowest in summer, while the western region (except Urumqi) shows the opposite feature. The features of monthly and quarterly variations also vary depending on the region under consideration. The monthly and quarterly variations in $NO_2$ in the Pearl River Delta are relatively moderate. In contrast, the change in the S. Hebei and N. Henan combined region and Jinan are clearly primarily due to excessive coal heating during wintertime. In addition, meteorological conditions have significant impacts influenced in different regions, especially in the Yangtze River Delta and Pearl River Delta. The higher temperature, larger amount of precipitable water and faster wind speed are all beneficial to $NO_2$ removal.

(4) In particular, Beijing and its surrounding areas show different characteristics of $NO_2$ variations. Beijing showed a significant downward trend during the 14-year study period. However, the Jing–Jin–Tang region showed the opposite tendency. For seasonal variations, conspicuous differences in $NO_2$ amount between Beijing and Jing–Jin–Tang occur in winter (January, February and December), and the values of the $NO_2$ columns in Beijing are basically smaller than those in Jing–Jin–Tang. The reasons for the different results are mainly because Beijing has implemented stricter environmental control policies.

Through the analysis of the spatial temporal variations in $NO_2$ VCD during the 14 studied years, the effectiveness of several environmental protection policies implemented in China are seen. In the future, the factors affecting the changes in $NO_2$ in different areas will be investigated in greater depth. Furthermore, specific control measures should be put forward according to different regions and different factors.

**Author Contributions:** C.W., T.W. and P.W. conceived and designed the experiments; C.W. collected and processed data; C.W. and T.W. analyzed and wrote the paper; and T.W. and P.W. contributed revisions to the paper.

**Funding:** This research was funded by the National Key R&D Program of China (Nos. 2017YFB0504000 and 2017YFC1501701) and the National Natural Science Foundation of China (No.41575034).

**Acknowledgments:** We thank NASA and KNMI for providing the OMI tropospheric $NO_2$ data used in this study (http://www.temis.nl).

**Conflicts of Interest:** The authors declare no conflict of interest.

## References

1. Kasibhatla, P.S.; Levy, I.H.; Moxim, W.J.; Chameidest, W.L. The relative impact of stratospheric photochemical production on tropospheric $NO_y$ levels: A model study. *J. Geophys. Res. Atmos.* **1991**, *96*, 18631–18646. [CrossRef]
2. Environmental Protection Agency. *Air Quality Criteria for Nitrogen Oxides*; Environmental Protection Agency: Washington, DC, USA, 1971.
3. Environmental Protection Agency. *Environmental Criteria and Assessment Office. Air Quality Criteria for Ozone and Other Photochemical Oxidants*; U.S. Environmental Protection Agency: Washington, DC, USA, 1978.
4. Barker, K.; Cambi, F.; Catcott, E.J.; Chambers, L.A.; Halliday, E.C.; Hasegawa, A.; Heimann, H.; Jammet, H.P.; Katz, M.; Leclerc, E.; et al. *Air Pollution*; World Health Organization: Geneva, Switzerland, 1961; Volume 437, pp. 40–45.
5. Celarier, E.A.; Brinksma, E.J.; Gleason, J.F.; Veefkind, J.P.; Cede, A.; Herman, J.R.; Ionov, D.; Goutail, F.; Pommereau, J.P.; Lambert, J.C.; et al. Validation of Ozone Monitoring Instrument nitrogen dioxide columns. *J. Geophys. Res. Atmos.* **2008**, *113*, D15S15. [CrossRef]
6. World Health Organization Regional Office for Europe. Air quality guidelines: Global update 2005. Particulate matter, ozone, nitrogen dioxide and sulfur dioxide. *Indian J. Med. Res.* **2007**, *4*, 492–493.
7. Boersma, K.F.; Eskes, H.J.; Brinksma, E.J. Error analysis for tropospheric $NO_2$ retrieval from space. *J. Geophys. Res. Atmos.* **2004**, *109*. [CrossRef]

8. Yienger, J.J.; Levy, H., II. Empirical model of global soil-biogenic $NO_x$ emissions. *J. Geophys. Res. Atmos.* **1995**, *100*, 11447–11464. [CrossRef]
9. Van der A, R.J.; Eskes, H.J.; Boersma, K.F.; van Noije, T.P.C.; Van Roozendael, M.; De Smedt, I.; Peters, D.H.M.U.; Meijer, E.W. Trends, seasonal variability and dominant $NO_x$ source derived from a ten year record of $NO_2$ measured from space. *J. Geophys. Res. Atmos.* **2008**, *113*. [CrossRef]
10. Heue, K.-P.; Richter, A.; Bruns, M.; Burrows, J.P.; Friedeburg, C.v.; Platt, U.; Pundt, I.; Wang, P.; Wagner, T. Validation of SCIAMACHY tropospheric $NO_2$-coloumns with AMAXDOAS measurements. *Atmos. Chem. Phys.* **2005**, *5*, 1039–1051. [CrossRef]
11. Schneider, P.; Lahoz, W.; van der A, R. Recent satellite-based trends of tropospheric nitrogen dioxide over large urban agglomerations worldwide. *Atmos. Chem. Phys.* **2015**, *15*, 1205–1220. [CrossRef]
12. Krotkov, N.A.; McLinden, C.A.; Li, C.; Lamsal, L.N.; Celarier, E.A.; Marchenko, S.V.; Swartz, W.H.; Bucsela, E.J.; Joiner, J.; Duncan, B.N.; et al. Aura OMI observations of regional $SO_2$ and $NO_2$ pollution changes from 2005 to 2015. *Atmos. Chem. Phys.* **2016**, *16*, 4605–4629. [CrossRef]
13. Wang, T.; Hendrick, F.; Wang, P.; Tang, G.; Clémer, K.; Yu, H.; Fayt, C.; Hermans, C.; Gielen, C.; Müller, G.F.; et al. Evaluation of tropospheric $SO_2$ retrieved from MAX-DOAS measurements in Xianghe, China. *Atmos. Chem. Phys.* **2014**, *14*, 11149–11164. [CrossRef]
14. Wang, T.; Wang, P.; Theys, N.; Tong, D.; Hendrick, F.; Zhang, Q.; Roozendael, M.V. Spatial and temporal changes in $SO_2$ regimes over China in the recent decade and the driving mechanism. *Atmos. Chem. Phys.* **2018**, *18*, 18063–18078. [CrossRef]
15. Streets, D.G.; Yarber, K.F.; Woo, J.H.; Carmichael, G.R. Biomass burning in Asia: Annual and seasonal estimates and atmospheric emissions. *Glob. Biogeochem. Cycles* **2003**, *17*, 1099. [CrossRef]
16. Wang, Y.X.; McElroy, M.B. Asian emissions of CO and $NO_x$: Constraints from aircraft and Chinese station data. *J. Geophys. Res. Atmos.* **2004**, *109*. [CrossRef]
17. The Multi-resolution Emission Inventory for China (MEIC). Available online: http://www.meicmodel.org/ (accessed on 28 July 2019).
18. Li, M.; Zhang, Q.; Kurokawa, J.I.; Woo, J.H.; He, K.; Lu, Z.; Ohara, T.; Song, Y.; Streets, D.G.; Carmichael, G.R. MIX: A mosaic Asian anthropogenic emission inventory under the international collaboration framework of the MICS-Asia and HTAP. *Atmos. Chem. Phys.* **2017**, *17*, 935–963. [CrossRef]
19. Velders, G.J.M.; Granier, C.; Portmann, R.W.; Pfeilsticker, K.; Wenig, M.; Wagner, T.; Platt, U.; Richter, A.; Burrows, J.P. Global tropospheric $NO_2$ column distributions: Comparing three-dimensional model calculations with GOME measurements. *J. Geophys. Res. Atmos.* **2001**, *106*, 12643–12660. [CrossRef]
20. Richter, A.; Burrows, J.P. Tropospheric $NO_2$ from GOME measurements. *Adv. Space Res.* **2002**, *29*, 1673–1683. [CrossRef]
21. Kostadinov, I.; Petritoli, A.; Werner, R.; Valev, D.; Atanasov, A.; Bortoli, D.; Markova, T.; Ravegnani, F.; Palazzi, E.; Giovanelli, G. Validation of SCIAMACHY $NO_2$ Vertical Column Densities with Mt. Cimone and Stara Zagora Ground-Based Zenith Sky DOAS Observations. In Proceedings of the Second Workshop on the Atmospheric Chemistry, Validation of Envisat (ACVE-2), ESA-ESRIN, Frascati, Italy, 3–7 May 2004.
22. Schaub, D.; Brunner, D.; Boersma, K.F.; Keller, J.; Folini, D.; Buchmann, B.; Berresheim, H.; Staehelin, J. SCIAMACHY tropospheric $NO_2$ over Switzerland: Estimates of $NO_x$ lifetimes and impact of the complex Alpine topography on the retrieval. *Atmos. Chem. Phys.* **2007**, *7*, 5971–5987. [CrossRef]
23. Blond, N.; Boersma, K.F.; Eskes, H.J.; van der A, R.J.; Van Roozendael, M.; De Smedt, I.; Bergametti, G.; Vautard, R. Intercomparison of SCIAMACHY nitrogen dioxide observations in situ measurements and air quality modeling results over Western Europe. *J. Geophys. Res. Atmos.* **2007**, *112*. [CrossRef]
24. Ialongo, I.; Hakkarainen, J.; Hyttinen, N.; Jalkanen, J.-P.; Johansson, L.; Boersma, K.F.; Krotkov, N.A.; Tamminen, J. Characterization of OMI tropospheric $NO_2$ over the Baltic Sea region. *Atmos. Chem. Phys.* **2014**, *14*, 7795–7805. [CrossRef]
25. Boersma, K.F.; Eskes, H.J.; Veefkind, J.P.; Brinksma, E.J.; van der A, R.J.; Sneep, M.; van den Oord, G.H.J.; Levelt, P.F.; Stammes, P.; Gleason, J.F.; et al. Near-real time retrieval of tropospheric $NO_2$ from OMI. *Atmos. Chem. Phys.* **2007**, *7*, 2103–2118. [CrossRef]
26. Bucsela, E.J.; Krotkov, N.A.; Celarier, E.A.; Lamsal, L.N.; Swartz, W.H.; Bhartia, P.K.; Boersma, K.F.; Veefkind, J.P.; Gleason, J.F.; Pickering, K.E. A new stratospheric and tropospheric $NO_2$ retrieval algorithm for nadir-viewing satellite instruments: Applications to OMI. *Atmos. Meas. Tech.* **2013**, *6*, 2607–2626. [CrossRef]

27. Griffin, D.; Zhao, X.; McLinden, C.A.; Boersma, F.; Bourassa, A.; Dammers, E.; Degenstein, D.; Eskes, H.; Fehr, L.; Fioletov, V.; et al. High-Resolution Mapping of Nitrogen Dioxide with TROPOMI: First Results and Validation over the Canadian Oil Sands. *Geophys. Res. Lett.* **2019**, *46*, 1049–1060. [CrossRef]
28. Zhang, Q.; Geng, G.; Wang, S.; Andreas, R.; He, K. Satellite remote sensing of changes in $NO_x$ emissions over China: 1996–2010. *Chin. Sci. Bull.* **2012**, *16*, 1446–1453.
29. Schneider, P.; van der A, R.J. A global single-sensor analysis of 2002–2011 tropospheric nitrogen dioxide trends observed from space. *J. Geophys. Res. Atmos.* **2012**, *117*. [CrossRef]
30. Geddes, J.A.; Martin, R.V. Global deposition of total reactive nitrogen oxides from 1996 to 2014 constrained with satellite observations of $NO_2$ columns. *Atmos. Chem. Phys.* **2017**, *17*, 1–44. [CrossRef]
31. Xiao, K.; Wang, Y.; Wu, G.; Fu, B.; Zhu, Y. Spatiotemporal Characteristics of Air Pollutants ($PM_{10}$, $PM_{2.5}$, $SO_2$, $NO_2$, $O_3$, and CO) in the Inland Basin City of Chengdu, Southwest China. *Atmosphere* **2018**, *9*, 74. [CrossRef]
32. Van der A, R.J.; Peters, D.H.M.U.; Eskes, H.; Boersma, K.F.; Van Roozendael, M.; De Smedt, I.; Kelder, H.M. Detection of the trend and seasonal variation in tropospheric $NO_2$ over China. *J. Geophys. Res. Atmos.* **2006**, *111*, 1–10. [CrossRef]
33. Zhang, X.; Zhang, P.; Zhang, Y.; Li, X.; Qiu, H. The variation trend and temporal-spatial distribution as well as the source analysis of tropospheric $NO_2$ in latest 10 years over China. *Sci. China D Earth Sci.* **2007**, *37*, 1409–1416.
34. Lin, J.T.; McElroy, M.B. Detection from space of a reduction in anthropogenic emissions of nitrogen oxides during the Chinese economic downturn. *Atmos. Chem. Phys.* **2011**, *11*, 8171–8188. [CrossRef]
35. Georgoulias, A.K.; Van der A, R.J.; Stammes, P.; Boersma, K.F.; Eskes, H.J. Trends and trend reversal detection in 2 decades of tropospheric $NO_2$ satellite observations. *Atmos. Chem. Phys.* **2019**, *19*, 6269–6294. [CrossRef]
36. Dirksen, R.J.; Boersma, K.F.; Eskes, H.J.; Ionov, D.V.; Bucsela, E.J.; Levelt, P.F.; Kelder, H.M. Evaluation of stratospheric $NO_2$ retrieved from the Ozone Monitoring Instrument: Intercomparison, diurnal cycle, and trending. *J. Geophys. Res. Atmos.* **2011**, *116*. [CrossRef]
37. Wang, T.; Wang, P.; Hendrick, F.; Yu, H.; Van Roozendael, M. The Spatial and Temporal Variability of Tropospheric $NO_2$ during 2005–2014 over China Observed by the OMI. *Atmos. Ocean. Sci. Lett.* **2015**, *8*, 392–396.
38. Liu, F.; Beirle, S.; Zhang, Q.; Van der A, R.J.; Zheng, B.; Tong, D.; He, K. $NO_x$ emission trends over Chinese cities estimated from OMI observations during 2005 to 2015. *Atmos. Chem. Phys.* **2017**, *17*, 9261. [CrossRef]
39. Hou, Y.; Wang, L.; Zhou, Y.; Wang, S.; Liu, W.; Zhu, J. Analysis of the tropospheric column nitrogen dioxide over China based on satellite observations during 2008–2017. *Atmos. Pollut. Res.* **2019**, *10*, 651–655. [CrossRef]
40. Xiao, Z.; Jiang, H.; Cheng, M. Characteristics of atmospheric $NO_2$ over China using OMI remote sensing data. *Acta Sci. Circumst.* **2011**, *31*, 2080–2090.
41. Van der A, R.J.; Mijling, B.; Ding, J.; Koukouli, M.E.; Liu, F.; Li, Q.; Mao, H.; Theys, N. Cleaning up the air: Effectiveness of air quality policy for $SO_2$ and $NO_x$ emissions in China. *Atmos. Chem. Phys.* **2017**, *17*, 1–18. [CrossRef]
42. Ai, J.; Sun, Y.; Zheng, F.; Ni, C.; Gui, K.; Zhang, X.; Jiang, W.; Liao, T. The spatial temporal variation and factor analysis of the tropospheric $NO_2$ columns in the Sichuan Basin from 2005 to 2016. *Atmos. Pollut. Res.* **2018**, *9*, 1157–1166. [CrossRef]
43. Cai, K.; Zhang, Q.; Li, S.; Li, Y.; Ge, W. Spatial–Temporal Variations in $NO_2$ and $PM_{2.5}$ over the Chengdu–Chongqing Economic Zone in China during 2005–2015 Based on Satellite Remote Sensing. *Sensors* **2018**, *18*, 3950. [CrossRef]
44. Li, Y.; Zheng, Y.; Liu, M.; Zheng, B.; Wang, T.; Tong, D.; Su, J.; Wang, P.; Lin, J.; Zhang, Q. Satellite-based observations of changes in nitrogen dioxides over the Beijing-Tianjin-Hebei region from 2011 to 2017. *Acta Sci. Circumst.* **2018**, *38*, 3797–3806.
45. Ma, Z.; Liu, R.; Liu, Y.; Bi, J. Effects of air pollution control policies on $PM_{2.5}$ pollution improvement in China from 2005 to 2017: A satellite-based perspective. *Atmos. Chem. Phys.* **2019**, *19*, 6861–6877. [CrossRef]
46. Notice of the Ministry of Environmental Protection on Issuing the General Planning for the Development of Environmental Protection Legislation and Environmental Economic Policies in China during the 12th Five-Year Plan Period. Available online: http://www.gov.cn/zwgk/2011-09/07/content_1941731.htm (accessed on 9 April 2019).

47. Notice of the Ministry of Environmental Protection on Issuing the General Planning for the Development of Environmental Protection Legislation and Environmental Economic Policies in China during the 13th Five-Year Plan Period. Available online: http://www.ndrc.gov.cn/gzdt/201701/t20170105_834501.html (accessed on 9 April 2019).
48. Clean Air Alliance of China. State Council Air Pollution Prevention and Control Action Plan, Issue II. Available online: http://en.cleanairchina.org/product/6346.html (accessed on 9 April 2019).
49. Levelt, P.F.; Veefkind, J.P.; Kroon, M.; Brinksma, E.J.; McPeters, R.D.; Labow, G.; Krotkov, N.; Ionov, D.; Hilsenrath, E.; Tamminen, J.; et al. The ozone monitoring instrument. *IEEE Trans. Geosci. Remote Sens.* **2006**, *44*, 1093–1101. [CrossRef]
50. Levelt, P.F.; Joiner, J.; Tamminen, J.; Veefkind, J.P.; Bhartia, P.K.; Stein Zweers, D.C.; Duncan, B.N.; Streets, D.G.; Eskes, H.J.; van der A, R.J.; et al. The Ozone Monitoring Instrument: Overview of 14 years in space. *Atmos. Chem. Phys.* **2018**, *18*, 5699–5745. [CrossRef]
51. Wenig, M.O.; Cede, A.M.; Bucsela, E.J.; Celarier, E.A.; Boersma, K.F.; Veefkind, J.P.; Brinksma, E.J.; Gleason, J.F.; Herman, J.R. Validation of OMI tropospheric $NO_2$ column densities using direct-Sun mode Brewer measurements at NASA Goddard Space Flight Center. *J. Geophys. Res. Atmos.* **2008**, *113*, 1–10. [CrossRef]
52. Bucsela, E.J.; Perring, A.E.; Cohen, R.C.; Boersma, K.F.; Celarier, E.A.; Gleason, J.F.; Wenig, M.O.; Bertram, T.H.; Wooldridge, P.J.; Dirksen, R.; et al. Comparison of tropospheric $NO_2$ from in situ aircraft measurements with near-real-time and standard product data from OMI. *J. Geophys. Res. Atmos.* **2008**, *113*, 1–14. [CrossRef]
53. Boersma, K.F.; Jacob, D.J.; Trainic, M.; Rudich, Y.; DeSmedt, I.; Dirksen, R.; Eskes, H.J. Validation of urban $NO_2$ concentrations and their diurnal and seasonal variations observed from the SCIAMACHY and OMI sensors using in situ surface measurements in Israeli cities. *Atmos. Chem. Phys.* **2009**, *9*, 3867–3879. [CrossRef]
54. Platt, U.; Stutz, J. *Differential Optical Absorption Spectroscopy: Principles and Applications*; Springer: Heidelberg, Germany, 2004.
55. Bucsela, E.J.; Celarier, E.A.; Wenig, M.O.; Gleason, J.F.; Veefkind, J.P.; Boersma, K.F.; Brinksma, E.J. Algorithm for $NO_2$ vertical column retrieval from the ozone monitoring instrument. *IEEE Trans. Geosci. Remote Sens.* **2006**, *44*, 1245–1258. [CrossRef]
56. Lamsal, L.N.; Krotkov, N.A.; Celarier, E.A.; Swartz, W.H.; Pickering, K.E.; Bucsela, E.J.; Gleason, J.F.; Martin, R.V.; Philip, S.; Irie, H.; et al. Evaluation of OMI operational standard $NO_2$ retrievals using in situ and surface-based $NO_2$ observations. *Atmos. Chem. Phys.* **2014**, *14*, 11587–11609. [CrossRef]
57. Ialongo, I.; Herman, J.R.; Krotkov, N.A.; Lamsal, L.N.; Boersma, K.F.; Hovila, J.; Tamminen, J. Comparison of OMI $NO_2$ observations and their seasonal and weekly cycles with ground-based measurements in Helsinki. *Atmos. Meas. Tech.* **2016**, *9*, 5203–5212. [CrossRef]
58. Tropospheric Emission Monitoring Internet Service. Available online: http://www.temis.nl (accessed on 28 July 2019).
59. Zhao, W.; Guo, J.; Yao, Z.; Yun, Y.; Jia, S.; Wang, W.; Zhang, P.; Xu, H.; Liu, H.; Gao, L.; et al. Declining hailstorm frequency in China during 1961–2015 and its potential influential factors. *Int. J. Climatol.* **2018**, *38*, 4116–4126. [CrossRef]
60. Chen, M.; Gong, Y.; Li, Y.; Lu, D.; Zhang, H. Population distribution and urbanization on both sides of the Hu Huanyong Line: Answering the Premier's question. *J. Geogr. Sci.* **2016**, *26*, 1593–1610. [CrossRef]
61. Wang, W.N.; Cheng, T.; Gu, X.; Chen, H.; Guo, H.; Wang, Y.; Bao, F.; Shi, S.; Xu, B.; Zuo, X.; et al. Assessing Spatial and Temporal Patterns of Observed Ground-level Ozone in China. *Sci. Rep.* **2017**, *7*, 3651. [CrossRef] [PubMed]
62. Wang, T.; Wang, P.; Yu, H.; Sun, L. Analysis of the characteristics of tropospheric $NO_2$ in Xianghe based on MAX-DOAS measurement. *Clim. Environ. Res.* **2014**, *19*, 51–60.
63. Yu, H.; Wang, P.; Zong, X.; Li, X.; Lv, D. Changes of $NO_2$ column Concentration during the Olympic Games in Beijing. *Chin. Sci. Bull.* **2009**, *54*, 299–304.
64. Diao, B.; Ding, L.; Su, P.; Cheng, J. The Spatial-Temporal Characteristics and Influential Factors of $NO_x$ Emissions in China: A Spatial Econometric Analysis. *Int. J. Environ. Res. Public Health* **2018**, *15*, 1405. [CrossRef] [PubMed]